11th International Symposium on Turbulence and Shear Flow Phenomena (TSFP11)
Southampton, UK, July 30 to August 2, 2019

TRANSPORT OF INERTIAL PARTICLES IN HIGH-RE TURBULENT BOUNDARY LAYER

Tim Berk
Department of Aerospace Engineering & Mechanics
St. Anthony Falls Laboratory
University of Minnesota
tberk@umn.edu

Filippo Coletti
Department of Aerospace Engineering & Mechanics
St. Anthony Falls Laboratory
University of Minnesota
fcoletti@umn.edu

ABSTRACT

Concentrations and velocities of small inertial particles in high-*Re* turbulent boundary layers (up to Re_τ = 19000) are measured via laser imaging. Three high-*Re* flows are combined with three particle sizes to give a range of parameters. Wall-normal profiles of streamwise velocity indicate that the particles slightly but consistently lag the fluid. The concentration profiles indicate a distinct wall-normal region where the Rouse profiles are followed, with significant deviations above and below this region. These deviations are compared to corrections of the Rouse profile. These corrections are made by starting from the advection-diffusion equation (as does Rouse) while making different assumptions. The deviations from Rouse away from the wall are qualitatively consistent with the introduction of a net flux, meaning that the advective flux is not perfectly balanced by the diffusive flux. The Rouse profile assumes this net flux equals zero. However, our data indicates this is not the case and indeed there is a relatively constant non-zero net flux. The deviations close to the wall are qualitatively consistent with a reduced mean settling velocity close to the wall. The Rouse profile assumes this settling velocity to be constant over the whole profile. A reduced settling velocity close to the wall could be caused by preferential sampling of the flow, by turbophoresis or by collisions of particles with the wall.

INTRODUCTION

The physics of inertial particles interacting with a turbulent boundary layer are of importance in a range of applications such as transport of pollen, snow, dust or sand in the atmospheric boundary layer, transport of granular materials and sediment in rivers as well as industrial and biological applications. Particle-turbulence interaction is typically described using a Stokes number ($St = \tau_p/\tau_f$), which gives the ratio between the particle response time (τ_p) and a relevant fluid time scale (τ_f). In homogeneous turbulence the Kolmogorov time scale ($\tau_\eta = (\nu/\varepsilon)^{1/2}$, where ν is the kinematic viscosity and ε is the turbulent dissipation) is generally used as the fluid time scale. The choice of fluid time-scale in turbulent boundary layers is less straightforward. The friction Reynolds number, $Re_\tau = \delta U_\tau/\nu$, where U_τ is the friction velocity and δ is the boundary-layer thickness, gives the ratio between the largest and smallest length-scales in a turbulent boundary layer. Using Re_τ the ratio between largest and smallest time scales in the flow can be written as $Re_\tau U_\tau/U_\infty$ where U_τ/U_∞ is a relatively constant function of $\log(Re_x)$ and typically $O(10^{-1})$. In the atmospheric boundary layer Re_τ is typically $O(10^6)$ (e.g. Hutchins *et al.* 2009), meaning that the time scales in the near-wall and outer regions differ by a factor $O(10^5)$. Therefore particles that may act as tracers in the outer layer could be ballistic in the near-wall region.

Computational studies often simplify the complex problem of inertial particles in the turbulent boundary layer. For very small particles, a common simplification is to negelect the effect of gravity, assuming negligible settling velocity. Another common simplification is the use of point-particles experiencing Stokes drag. Most experimental and computational studies have considered relatively low Reynolds number turbulent boundary layers ($Re_\tau \approx O(10^2)$), limiting the separation between time-scales in the inner and outer parts of the boundary layer.

In the present study we experimentally investigate the interaction of microscopic glass spheres with a turbulent boundary layer. The solid-to-fluid density ratio of $O(10^3)$ is representative of sand and dust in the atmosphere. The particles have mean diameters of d_p = 30, 50 and 100 μm, which is comparable to the viscous wall units. The Reynolds number is $Re_\tau \approx O(10^4)$ which is lower than but approaching regimes found in the atmospheric surface layer.

Concentration profiles

One of the characteristics influenced by the interaction between the particles and the turbulence is the wall-normal profile of particle concentration. This profile is usually considered to be driven by a balance between gravitational settling and turbulent dispersion (Rouse 1937, Richter & Chamecki 2018). This balance can be written as

$$C\, v_s - \varepsilon_y\, \partial C/\partial y = \Phi \qquad (1)$$

where C is the concentration, v_s is the time-averaged vertical particle velocity, ε_y is the turbulent diffusivity, y is the wall-normal height and Φ is the net flux. It is important to note that we define the vertical velocity as positive upwards. In the following we always assume a mean downward settling velocity, $v_s < 0$. Using Monin-Obukhov similarity theory, the turbulent diffusivity in turbulent boundary-layers is typically modelled as $\varepsilon_y = \kappa U_\tau y$ where $\kappa \approx 0.40$ is the von Kármán constant.

If the advective flux ($C\, v_s$) is perfectly balanced by the diffusive flux ($\varepsilon_y\, \partial C/\partial y$) there is a zero net flux ($\Phi = 0$). If we then assume v_s to be independent of y and the turbulent diffusivity of the particles to equal the turbulent diffusivity of the flow, Equation 1 can be integrated as

$$C/C_r = (y/y_r)^{Ro} \qquad (2)$$

where $Ro = v_s/\kappa U_\tau$ is the Rouse number and C_r and y_r are a reference concentration and reference height respectively. Using this power law, the logarithm of the concentration profile equals $\log(C/C_r) = Ro\, \log(y/y_r)$, indicating that when plotted on logarithmic axes the concentration profile has a constant slope given by Ro. Note that for a downward settling velocity $Ro < 0$,

meaning that as y increases C_r decreases. Equation 2, known as the Rouse concentration profile (often in modified form for open channel flow), is widely used to predict particle concentration profiles. However, the derivation of this Rouse profile relies on multiple assumptions of which the accuracy differs per case.

The first assumption is the perfect balance between the advective and diffusive fluxes, leading to a zero net flux $\Phi = 0$. The advective flux is driven by the local concentration and local mean velocity, while the diffusive flux is driven by the local turbulent diffusivity and the local concentration gradient. There is no obvious reason to assume the two are equal and therefore there is no reason to assume $\Phi = 0$ (Kind 1992). Incorporating a constant non-zero flux Φ in the integration of Equation 1 leads to a concentration profile given by

$$C/C_r = (1 - \Phi/\Phi_r)(y/y_r)^{Ro} + \Phi/\Phi_r \qquad (3)$$

where $\Phi_r = v_s C_r$ is a reference flux. The normalized flux Φ/Φ_r is negative when the diffusive flux is larger than the advective flux and positive when the advective flux is larger. Close to the wall $(y/y_r)^{Ro} >> \Phi/\Phi_r$ and the concentration profile is altered (compared to the one given by Equation 2) by a multiplicative constant: $C/C_r \approx (1 - \Phi/\Phi_r)(y/y_r)^{Ro}$. However, far away from the wall $(y/y_r)^{Ro} << \Phi/\Phi_r$ and the concentration profile is dominated by the non-zero flux, $C/C_r \approx \Phi/\Phi_r$. Note that in the derivation of Equation 3 it was assumed that the particle flux is constant, while this does not have to be the case. In fact, when there is no deposition (or erosion) of particles at the surface, the flux at the surface is zero, meaning that for non-zero flux away from the wall, the flux varies with y.

The second assumption is the modeling of turbulent diffusivity of particles as $\varepsilon_y = \kappa U_\tau y$. While this is fairly well established for turbulent boundary layers, for inertial particles this formulation is expected to be an approximation. The similarity of the particle diffusivity to the diffusivity of the flow is expected to depend on the Stokes number. The particle dispersion in a turbulent boundary layer is not well understood and is part of our ongoing investigation.

The third assumption is that the particle velocity is independent of y. Typically this is taken equal to the particle settling velocity in a quiescent fluid, which is approximated by $v_s = \tau_p g$ where g is the gravitational acceleration, but numerous studies have shown that the settling velocity may be different in turbulent flows. Changes to the mean particle velocity include (but are not limited to) preferential sampling of the flow (e.g. Wang and Maxey, 1993) and turbophoresis (e.g. Richter & Chamecki 2018). Both effects can be assumed to vary with wall-normal height and make the particle velocity dependent of y. In addition, collisions with the wall affect the mean vertical velocity near the wall. If these collisions are assumed to be elastic (i.e. no loss of kinetic energy) the upward velocity of the particles (immediately after colliding with the wall) equals the downward velocity (immediately before colliding) and the net velocity at the wall equals zero. Instead, if we assume a non-unity coefficient of restitution ($e = -v_{up}/v_{down}$, where v_{down} and v_{up} denote the velocities just before and just after the collision respectively) we get a net velocity at the wall of $v_{wall} = v_{down}(1-e)$. If for simplicity we neglect the dependency of v_s on y in the derivation of Equation 2 and instead just consider a smaller v_s at the wall due to inelastic collisions, the slope of the Rouse profile (given by the Rouse number $Ro = v_s/\kappa U_\tau$) decreases near the wall.

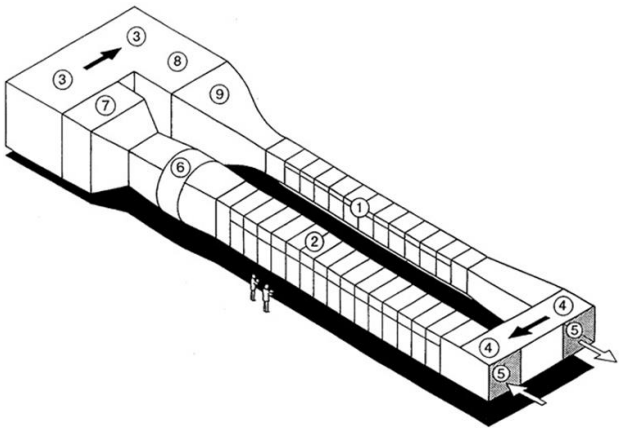

Figure 1. Atmospheric boundary layer wind tunnel

The changes to the assumptions made in the derivation of the Rouse profile as discussed above lead to a different shape of the concentration profile. In the present study the concentration profiles of inertial particles in a turbulent boundary layer are investigated experimentally. Measured concentration profiles are compared to the Rouse profile predicted by Equation 2 as well as to profiles modelled using the discussed changes to the Rouse profile.

EXPERIMENTAL METHODS

Experiments are performed in the atmospheric boundary layer wind tunnel at the St. Anthony Falls Laboratory, University of Minnesota. A schematic of this closed-loop facility is provided in Figure 1. The test-section used in this study is section 1 as indicated in the schematic, which is 16 m long and has a cross-section of 1.7 by 1.7 m. We use x, y and z to denote streamwise, wall-normal, and spanwise directions, respectively. Measurements are performed at free-stream velocities of U_∞ = 5, 10 and 15 m/s. The boundary layer is tripped at the leading edge of the test section using a picket-fence type boundary layer trip, leading to boundary-layer thicknesses of δ = 0.57 m (U_∞ = 5 m/s) and δ = 0.53 m (U_∞ = 10 and 15 m/s) at the measurement location 12.5 m downstream of the trip. This yields friction-velocity Reynolds numbers of Re_τ = 7000, 13000 and 19000 for increasing free-stream velocities.

Single-phase measurements

The unladen flow is seeded using olive-oil droplets, injected into the contraction of the wind tunnel (section 9 in Fig. 1) and velocity fields are obtained over the streamwise/wall-normal plane at mid-span using particle image velocimetry (PIV). The flow is illuminated using a Big Sky dual-pulse 200 mJ Nd:YAG laser. Two TSI Powerview 4MP cameras are used to take wall-normal profiles up to y = 0.72 m with a resolution of 1.3 mm per vector. Wall-normal profiles of the mean and fluctuating streamwise velocity components are compared against a canonical case (Hutchins *et al.* 2009) in Figure 2. The mean velocity profile (a) shows a deviation from the canonical case in the wake-region, visible at $y^+ > 10^3$. Where in the canonical case a strong wake region is present (defined as deviation from the log-law), in our facility the wake-strength seems to be negligible. Such an absence of the wake has been linked to an increase in turbulent activity, caused for example by increased free-stream turbulence intensity (see e.g. Sharp 2009) or by the tripping condition (see e.g. Rodríguez-López 2016). It is assumed that the absence of

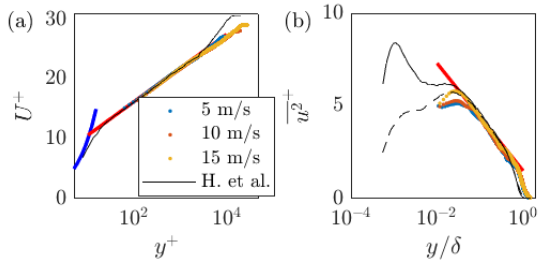

Figure 2. Unladen flow profiles for Re_τ = 7000, 13000 and 19000 respectively, compared to Re_τ = 14000 from *Hutchins et al.* (2009). The dashed line corresponds to underresolved velocity fluctuations for Re_τ = 14000 (l^+ = 153 hot-wire).

Table 1. Parameters for the cases used in this study.

d_p (µm)	U_∞ (m/s)	d^+	St^+	Ro
30	5	0.4	18.3	-0.93
30	10	0.7	65.7	-0.49
30	15	1.1	137.0	-0.34
50	5	0.7	45.0	-2.14
50	10	1.2	150.9	-1.13
50	15	1.8	314.8	-0.78
100	10	2.5	417.1	-3.12
100	15	3.6	870.2	-2.16

the wake is a combination of a relatively high free-stream turbulence and the tripping condition. In the near-wall and logarithmic region both the mean (U^+) and fluctuating (u^{2+}) velocity components are similar to the canonical case. Note that due to the spatial resolution of PIV the small near-wall velocity fluctuations cannot be resolved and an attenuation is visible in Fig. 2b for $y/\delta < 3{\cdot}10^{-3}$. This resolution issue is similar to the case of using a relatively large hot-wire (the dashed black line in Fig. 2b taken in the same facility as the solid black line). Inertial-particle measurements focus on the near-wall region (roughly $y/\delta < 10^{-1}$) where the boundary layer is similar to the canonical turbulent boundary layer.

Two-phase measurements

Inertial particles (glass spheres with diameters of d_p = 30, 50 and 100 µm) are seeded into the boundary layer for all three flow velocities. The three flow velocities in combination with three particle types give a matrix of nine cases. However, the largest particles (100 µm) in the slowest flow (5 m/s) do not remain suspended and settle on the floor. Therefore, this case is omitted. The eight cases are listed in Table 1. A set of non-dimensional parameters is given for each case. These are $d^+ = d_p U_\tau/\nu$, $St^+ = \tau_p U_\tau^2/\nu$ and $Ro = \nu_s/\kappa U_\tau$. The particles are introduced in the flow 1.2 m downstream of the trip using an airfoil to guide the seeding tube as shown in Figure 3. The tube has a diameter of D = 0.01 m and is located x_j = 1130D upstream of the measurement location. A particle-air mixture is injected into the flow in streamwise direction. It is assumed the jet is far enough upstream such that (i) the fluid phase has a negligible effect on the measured flow and (ii) the seeding gets mixed with the flow in the boundary layer. The first assumption is verified by comparing the flow velocity in the single-phase measurements to the fluid velocity in the multi-phase measurements as presented in Figure 4. Differences are negligible, indicating that the injection of the particle-air mixture does not alter the (mean) flow. Filters are placed

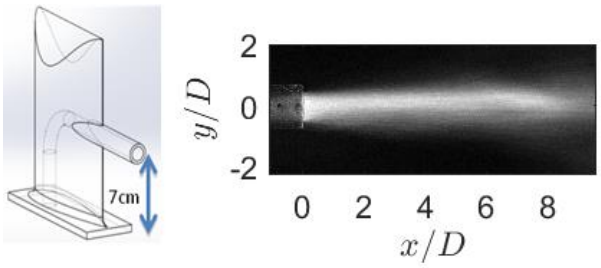

Figure 3. Schematic and instantaneous image (at 5 m/s) of particle injection.

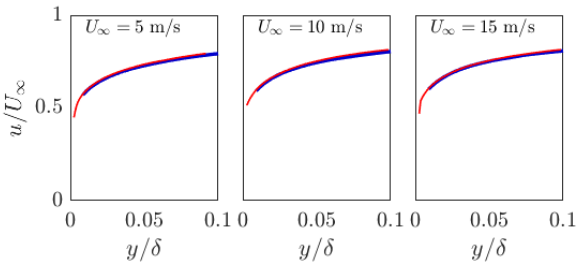

Figure 4. Comparison of flow velocity in single-phase measurements (blue lines) to flow velocity in multi-phase measurements (red lines) for representative cases.

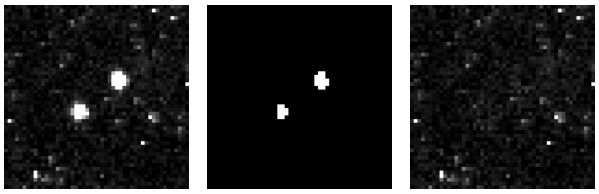

Figure 5. Sample of the raw data for a case with d_p = 50 µm particles. Panel a shows the recorded data. Panels b and c show the particle and tracer fields for the same window respectively.

downstream of the test section to prevent inertial particles from re-entering the test section after looping through the tunnel. It is checked that these filters have a negligible effect on the mean and fluctuating velocity profiles as well as on the pressure gradient in the test section.

During the multiphase measurements the flow is seeded with tracers to enable simultaneous PIV and particle tracking velocimetry (PTV). The same laser and cameras are used as during the single-phase measurements. The cameras are placed side-by-side (in streamwise direction) to increase convergence of particle measurements. The cameras are fitted with 200 mm lenses to capture a field of view of 59 mm in streamwise direction and 53 mm in wall-normal direction (starting at the bottom wall). The resolution of 32 pixels/mm gives inertial particle images with diameters of approximately 5-12 pixels (depending on the particle size), making it possible to determine a sub-pixel location of each particle. A 50 by 50 pixels sample of a raw image is shown in Figure 5a. This sample corresponds to the case with d_p = 50 µm, U_∞ = 5 m/s.

Processing algorithm

In-house PIV and PTV algorithms are used (discussed in more detail in Petersen *et al.*, 2019). The algorithm first separates the raw images into a particle field and a tracer field.

Inertial particles are identified in the raw images based on size and intensity of connected groups of pixels. The tracer field is obtained by removing the inertial particles from the raw images. In the tracer field locations that previously contained inertial particles are filled up with Gaussian noise such that the PIV cross-correlation is not biased by the holes left by the removal of the inertial particles. An example of this separation is given in Figure 5 where the extracted particle field (panel b) and tracer field (panel c) are presented next to a sample of raw data (panel a). Multi-pass PIV is used on the tracer field to obtain instantaneous fluid-phase velocities. In the particle field, the algorithm identifies particles as groups of pixels above specified intensity and size thresholds. Particles are then matched between the images in each pair by searching for particles in a given search radius outside the displacement expected from the instantaneous fluid velocity. This gives a location and velocity for each matched particle pair. The accuracy of the measured particle velocity is highly dependent on the particle displacement. There is a large difference between the streamwise and wall-normal particle displacements. This is approximately shown by the ratio v_s/U_∞, which ranges from 0.5% to 5% (depending on the case), indicating that while our streamwise velocities are accurate our wall-normal velocities may be inaccurate. Wall-normal profiles of concentration and velocity are determined by binning particles based on wall-normal location. Given the expected logarithmic variation of concentration (Equation 2), bin sizes are increased logarithmically with distance from the wall such that the number of particles per bin stays relatively constant. Per run, both cameras record 1000 images. Two runs are performed per case, leading to data sets of 2000 image pairs. Depending on the case, these images contain a total of $O(10^5$ - $10^6)$ detected particles.

RESULTS

Wall-normal profiles of streamwise velocities are presented in Figure 6. Particle velocities for the d_p = 30 (red lines), 50 (green lines) and 100 µm particles (blue lines) are compared to the mean fluid velocity (black lines). In general, the mean streamwise particle velocity follows the mean flow velocity, but with a consistent lag. This is in agreement with the trend reported in a water flow by Kiger & Pan (2002). Away from the wall, the lag increases with particle size. This trend is reversed close to the wall where the largest particles have the smallest lag and are possibly even faster than the flow. This could be caused by the ability of the larger (more inertial) particles to bring momentum from the outer parts of the boundary layer down towards the wall.

Unscaled wall-normal profiles of volume fraction are presented in Figure 7. Volume fractions are generally lower than $\varphi_v = 10^{-5}$ (except close to the wall for the 100 µm particles), suggesting one-way coupled regimes.

Normalized concentration distributions are presented in Figure 8 for all cases. Overlaid on this figure are the concentration profiles predicted by the Rouse profile (Equation 2, dark lines). Rouse numbers are calculated using a settling velocity based on a particle-response time using Schiller & Naumann correction (Clift *et al.* 2005). The reference concentration C_r is taken at a constant height in the wall-normal profile (y_r/δ = 0.02). This reference height is chosen as the height for which the Rouse profile best matches the measured concentration profiles. In general, the middle of the profiles (around y/y_r = 1) is predicted reasonably well by Equation 2. An exception are the two cases with d_p = 100 µm

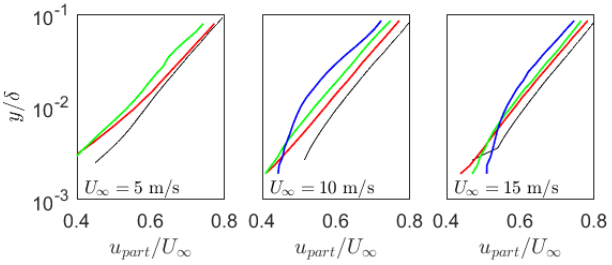

Figure 6. Wall-normal profiles of streamwise velocity for the fluid phase (black lines) compared to the particle velocities for the 30 µm particles (red lines), 50 µm particles (green lines) and 100 µm particles (blue lines).

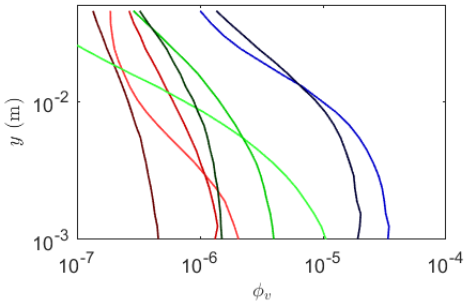

Figure 7. Wall-normal profiles of volume fraction for d_p = 30 (red lines), 50 (green lines) and 100 µm (blue lines). Darker colors indicate larger flow velocities.

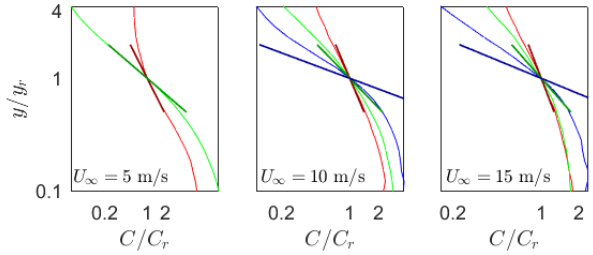

Figure 8. Wall-normal concentration profiles for for d_p = 30 (red lines), 50 (green lines) and 100 µm (blue lines), compared to slopes as predicted by the Rouse profile (Equation 2) given by the dark lines.

particles for which the predicted Rouse number seems too large by roughly a factor 1.6. Assuming that the Rouse profile is accurate in this part of the boundary layer, this deviation could be due to an overprediction of the particle settling velocity in the Rouse number or an underprediction of the friction velocity. The friction velocity in this case might be altered by the larger volume fraction (compared to the other cases) near the wall as presented in Figure 7. A change in the fluid velocity could not be measured. Given the constant deviation for both cases using the d_p = 100 µm particles, it is likely that their settling velocity is different than expected. The settling velocity for these particles can be overpredicted due to the used simplifications to estimate v_s as discussed above. Alternatively, other assumptions leading to Equation 2 as discussed above might be invalid for these two cases, which would explain the deviation from the predicted slope.

The constant slope around y/y_r = 1 for the concentration profiles in Figure 8 changes near the wall as well as further away from the wall. The deviation away from the wall is not

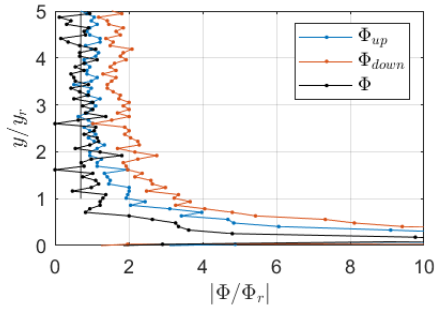

Figure 9. Particle flux normalized by $\Phi_r = v_s C_r$ for the case of U_∞ = 5 m/s, d_p = 30 µm. The net flux is downward.

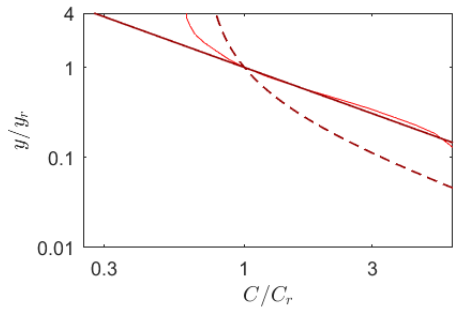

Figure 10. Measured concentration profile for the case of U_∞ = 5 m/s, d_p = 30 µm compared to the Rouse profile given by Equation 2 (solid dark line) and compared to the profile given by Equation 3 (dashed dark line).

visible for all cases, which could be caused by the limited wall-normal extent of the profiles. In both regions the slope (defined as dC/dy) increases.

The deviation away from the wall (y/y_r > 1) is most pronounced for the case of U_∞ = 5 m/s, d_p = 30 µm. As discussed above, a deviation away from the wall could be caused by a non-zero net flux. The particle flux for the U_∞ = 5 m/s, d_p = 30 µm case is measured by counting the particles traveling through a given plane. The time-averaged particle flux is presented in Figure 9. The net flux is determined as $\Phi = \Phi_{up} - \Phi_{down}$. Note that in this figure the absolute value of the three fluxes is given for comparison, but the net flux is downward. Regardless of the uncertainty in the measured vertical particle displacements, the fluxes in Figure 9 show a clear trend. Both the upward and downward fluxes are roughly constant away from the wall and increase sharply close to the wall. The increase near the wall can be expected from the increased concentration. The net flux for y/y_r > 1 is roughly equal to Φ/Φ_r = 0.7 as indicated by the vertical line. Using this measured flux, a correction to the Rouse profile can be made using Equation 3. This correction is plotted in Figure 10, along with the measured concentration profile and the Rouse profile given by Equation 2. Note that the constant flux used for this correction is only valid for y/y_r > 1. The profile is extended towards the wall for comparison to the Rouse slope. The slope (dC/dy) of the correction (dashed line) goes down for y/y_r > 1, similar to the measured case, while tending towards the slope in the Rouse profile for y/y_r << 1. It is clear that the dashed line in Figure 10 over-corrects the concentration profile. This is possibly caused by the uncertainty in the determination of the net-flux as evident from the noise in Figure 9 or by other incorrect simplified assumptions made in the derivation of

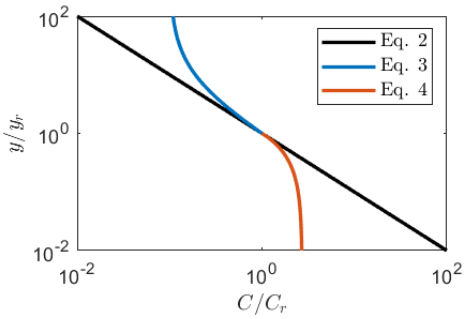

Figure 11. Concentration profiles as predicted by Eq. 2, Eq. 3 (for $y > y_r$) and Eq. 4 (for $y < y_r$) with Ro = -1 and Φ/Φ_r = 0.1.

Equations 2 and 3. The important result here is the observation that a net downward flux can alter the Rouse profile away from the wall in a matter qualitatively similar as seen in the measured profiles.

In addition to a deviation from the Rouse slope away from the wall in Figure 8, the concentration profiles all deviate from the Rouse slope close to the wall (y/y_r < 1). Slopes near the wall decrease compared to the Rouse prediction. Using the slope as predicted by Equation 2 this would indicate a lower Rouse number $Ro = v_s/\kappa U_\tau$ close to the wall. This could be caused by either a decrease in mean vertical velocity, or an increase in friction velocity. Hypothetically an increase in friction velocity might be caused by the pressence of particles near the wall. However, for some cases the volume fraction stays below $\varphi_v = 10^{-6}$ as presented in Figure 7, which would make it unlikely that the flow properties are altered by the particles. The mean vertical particle velocity might be reduced near the wall, thereby lowering the Rouse number and decreasing the slope of the concentration profile. The particle velocity could be reduced by preferential sampling of the flow or by turbophoresis. Turbophoresis transports particles down a slope of velocity fluctuations. If we assume that the wall-normal profile of particle velocity fluctuations is qualitatively similar to fluid velocity fluctuations this transport would be away from the wall in our measurement domain. In addition, particles with a downward velocity near the wall are likely to collide with the wall and bounce back. This also reduces the mean downward velocity component. These reductions in mean particle settling velocity near the wall would qualitatively explain the reduction in the slopes of the concentration profiles.

However, it is important to note that the derivation of the concentration profile in Equation 2 (and Eq. 3) is based on integration of Equation 1 over dy where it is assumed that v_s is constant. As an example, we can consider a case where the settling velocity v_s decreases linearly from a constant value v_r at $y \geq y_r$ to zero at the wall, i.e. $v_s = v_r\, y/y_r$ for $y < y_r$. Integration of Equation 1 (for Φ = 0) then yields

$$C/C_r = \exp(Ro(y/y_r - 1)) \qquad (4)$$

Note that the reference height y_r has a different physical meaning in Equations 2, 3 and 4. Whereas Equation 2 is qualitatively independent of the reference height, in Equation 3 y_r sets the strength of the correction, since $\Phi_r = v_s C_r = v_s C(y_r)$ and in Equation 4 y_r sets the start of the hypothetical linear decay of the wall-normal particle velocity. Concentration profiles predicted by Equations 2, 3 and 4 are presented in Figure 11. These profiles all have Ro = -1, Φ/Φ_r = 0.1 and the

same y_r. The corrections given by Equations 3 and 4 qualitatively reflect the deviations from the Rouse profile observed in Figure 8 in the regions away from the wall (Eq. 3) and close to the wall (Eq. 4). It is important to note that even these corrections rely on simplified assumptions (i.e. a constant flux and a linearly decaying velocity profile respectively). The wall-normal extent for which the measured concentration profiles in Figure 8 follow the Rouse profile seems larger than in Figure 11. This can be easily adjusted by using a separate reference height in Equation 4 (e.g. $v_s = v_r\, y/(0.1\, y_r)$).

CONCLUSIONS

Experiments of inertial particles in high-Reynolds number turbulent boundary layers have been performed. Wall-normal profiles of the particle velocity and concentration have been presented. It is shown that while a region exists in which the concentration profile follows the Rouse profile, there are significant deviations from this profile close to the wall and further away from the wall. Corrections to the Rouse profile are presented by integrating the advection-diffusion equation using different assumptions. It is shown that a set of corrections can (qualitatively) explain the deviations to the Rouse profile. The deviation close to the wall is consistent with a decrease in particle settling velocity near the wall. This could be caused by (a combination of) preferential sampling, turbophoresis, collisions with the wall, or other mechanisms. The deviation from the Rouse profile further away from the wall is consistent with the introduction of a net downward flux of particles. This flux indicates that the advective flux and the diffusive flux in the advection-diffusion equation are not perfectly balanced as is typically assumed. Such a non-zero flux has been measured in our data.

Multiple assumptions remain in the derivation of the presented corrections to the Rouse profile. These include the mixing length model for turbulent diffusivity and the dependency of wall-normal particle velocity and flux on wall-normal location. These assumptions require further assessment in future studies.

REFERENCES

R. Clift *et al.*, *Bubbles, Drops and Particles*, (Academic Press, Inc. 1978)

N. Hutchins *et al.*, "Hot-wire spatial resolution issues in wall-bounded turbulence", *J. Fluid Mech.* **635**, 103 (2009)

K.T. Kiger and C. Pan, "Suspension and turbulence modification effects of solid particulates on a horizontal turbulent channel flow", *J. Turbulence* **3**, 019 (2002)

R.J. Kind, "One-dimensional aeolian suspension above beds of loose particles—a new concentration-profile equation", *Atmo. Env*. **26A**, 927 (1992)

A.J. Petersen *et al.*, "Experimental study of inertial particles clustering and settling in homogeneous turbulence", *J. Fluid Mech.* **864**, 925 (2019)

D. Richter and M. Chamecki, "Inertial effects on the vertical transport of suspended particles in a turbulent boundary layer", *B-L Meteorol.* **167**, 235 (2018)

E. Rodríguez-López *et al.*, "On the formation mechanism of artificially generated high Reynolds number turbulent boundary layers", *B-L Meteorol.* **160**, 201 (2016)

H. Rouse, "Modern conceptions of the mechanics of turbulence", *Trans. Am. Soc. Civ. Eng.* **102**, 436 (1937)

N.S. Sharp *et al.*, "Effects of large-scale free stream turbulence on a turbulent boundary layer", *Phys. Fluids* **21**, 095105 (2009)

L-.P. Wang and M.R. Maxey, "Settling velocity and concentration distribution of heavy particles in homogeneous isotropic turbulence", *J. Fluid Mech.* **256**, 27 (1993)